

G,3 · DEPARTURES FROM IDEAL PERFORMANCE

mentioned. This is logical since flight performance depends directly on I_{sp} , and only indirectly on η .

Consideration of the thermal efficiency leads to the idea of a heat balance for the rocket motor. The chemical energy introduced with the injected propellants is distributed in four directions: (1) a small part (up to 15 per cent) remains unconverted due to incomplete reaction; (2) about 1 per cent, more or less, of the heat reaction is transferred to the motor walls where it may be lost unless the motor is cooled by the liquid propellant (regenerative cooling); (3) the kinetic energy of the jet comprises a large part, from one third to two thirds, of the heat of reaction; and (4) finally, the remainder of the reaction heat is carried away in the hot jet as thermal energy.

Typical values of the performance parameters of rocket motors in the moderate and high performance classes, respectively, are indicated in Table G,2. It is notable that the flame temperatures range from 2000

Table G,2. Typical performance characteristics.

Performance parameter	Ordinary range	High range
T_c	2000–3000°K	3000–5000°K
c^*	4000–5500 ft/sec	5000–8000 ft/sec
C_F	1.3–1.5	1.5–1.6
I_{sp}	200–270 lb-sec/lb	270–400 lb-sec/lb
$\frac{W}{\dot{W}}$	20–25	8–20
γ	1.15–1.25	1.15–1.20

to 5000°K, and that dissociation is prominent in most of the range. The effects of dissociation constitute the greatest source of inaccuracy in the application of the ideal analysis just presented to actual rocket processes. The modification of the ideal analysis to handle dissociation will be discussed in Art. 4. Modifications due to other departures from the ideal conditions of this analysis are discussed in the following article.

G,3. Departures from Ideal Performance. The preceding ideal performance analysis requires correction to take care of the following actual conditions:

- a. Conical divergence of the exhaust jet.
- b. Surface friction and flow disturbances in the exhaust nozzle.
- c. Constriction of the exit area due to boundary layer build-up.
- d. Jet detachment.
- e. Heat loss from the hot gas to the cold motor walls.
- f. Suspended liquid or solid particles in the exhaust jet.
- g. Pressure drop in the combustion chamber due to heat release.

Consideration of the effects of temperature dependence of the specific heats and of chemical reaction during the expansion in the nozzle will be postponed until Art. 4.

The effect of exhaust nozzle divergence. A loss in thrust occurs as a result of the divergence of the exhaust jet as it leaves the nozzle, in comparison with the ideal case of parallel flow. The loss may be viewed as the decrease in the axial component of momentum due to the outward inclination of the streamlines. Inasmuch as the loss is usually only a few per cent, a fairly approximate theory is adequate to determine its magnitude.

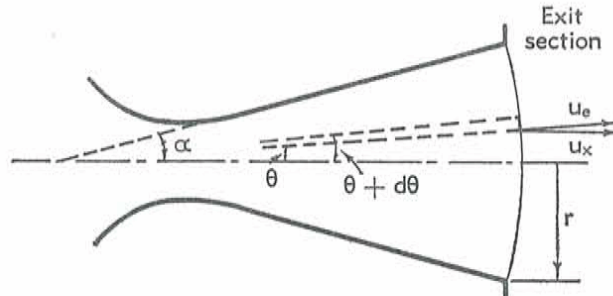


Fig. G,3a. Radial flow in exhaust nozzle.

If the exit-to-throat area ratio ϵ is sufficiently large, say at least 3, and if the half angle α of the exit cone is sufficiently small, say not more than 20° , it is reasonable to assume a radial flow pattern in the exhaust cone with concentric spherical caps for isobaric surfaces. The exit cone defines the location of the effective center for this radial flow pattern. The axis of the nozzle corresponds to $\theta = 0$, and the surface of the exit cone corresponds to $\theta = \alpha$ (Fig. G,3a).

To calculate the thrust, divide the exit flow area into differential annular areas between θ and $\theta + d\theta$. The axial component of the thrust of this element of flow is

$$dF = \rho_e V_e (2\pi r \sin \theta \cdot r d\theta) (V_e \cos \theta) + (p_e - p_\infty) (2\pi r \sin \theta \cdot r d\theta) \cos \theta$$

Integrating with respect to θ from 0 to α , F becomes

$$F_\alpha = \left(\frac{1 + \cos \alpha}{2} \right) [\dot{m} V_e + (p_e - p_\infty) A'_e] \quad (3-1)$$

In this formula, V_e , p_e , and A'_e come out in the analysis to be the velocity, pressure, and area of the *spherical isobaric cap* at the exit, and not the planar area at the exit. The quantity in brackets is the thrust of a zero divergence motor whose exit area equals A'_e . However, for small angle α , the planar exit area A_e is so close to A'_e that the thrust of the zero divergence motor would be almost unaffected if A'_e were replaced by A_e , and V_e and p_e were interpreted to apply to A_e instead of

A'_e . Therefore, if F_0 is the thrust of a zero divergence motor having an exit area ratio ϵ equal to the *planar* exit area ratio of the α divergence motor,

$$F_\alpha = \lambda F_0, \quad \text{where } \lambda = \frac{1}{2}(1 + \cos \alpha) \quad (3-2)$$

For $\alpha = 10^\circ$, $\lambda = 0.992$, and for $\alpha = 20^\circ$, $\lambda = 0.970$. Consequently, the correction is a small one, and the preceding simplified model for the flow field is justified. To measure the loss accurately in order to check the theory requires experiments of high precision. Some experimental results have been reported, which show that the formula (Eq. 3-2) holds reasonably well from $\alpha = 10^\circ$ to $\alpha = 30^\circ$. For smaller angles, the nozzles are so long that frictional losses dominate the results, and for angles in excess of 40° there is clear evidence of flow separation.

The most commonly employed divergence angle in practice is about 15° . This produces a loss of only 1.7 per cent, yet the nozzle is not so long as to be excessive in either weight or length. It is possible to design an exit section with a curved contour so as to produce a parallel jet and thereby recover this divergence loss, but the penalties of complexity and cost must then be accepted. For a design to produce the utmost in performance, e.g., a satellite launcher, this is worthwhile.

The effects of fluid friction and flow losses. It is not possible to calculate reliably the thrust loss due to surface friction, because so little is known of the nature of the boundary layer under the conditions of pressure gradient and curvature that exist in the nozzle. Also, the flow field in a practical nozzle is likely to exhibit strong pressure waves originating in the sharply curved region near the throat. The rocket designer ordinarily cannot eliminate such sharp curvature, as can the supersonic wind tunnel designer, because rocket nozzles must be made cheaply (hence simply) and must be compact. Consequently, the flow disturbances are accepted as long as the loss in thrust is small. Fortunately, it seems that drastically poor design is necessary to cause a thrust loss greater than, say 10 per cent, due to bad flow, and if the designer merely uses his French curves with good technique, the loss can be cut to about 1 or 2 per cent.

For example, if the nozzle contour consists of a converging cone of 30° half angle, a diverging cone of 15° half angle, and a throat section with a longitudinal radius of curvature equal to twice the radius of curvature of the throat section, the loss will ordinarily not exceed 3 per cent and will probably be nearer to 1 per cent if there are no sharp corners.

In test results, this type of loss is reported in the form of a discharge coefficient C_d that normally lies between 0.97 and 0.99.

$$(C_F)_{\text{actual}} = C_d \lambda [(C_F)_{\alpha=0}]_{\text{ideal}} \quad (3-3)$$

Constriction of the exit area by the boundary layer. The effect of the boundary layer in constricting the flow passage of the nozzle can be con-

sidered in two places, at the throat and at the exit. At the throat, a boundary layer would reduce the mass flow \dot{m} ; at the exit, it would reduce the effective expansion by reducing ϵ . It turns out that the first effect is negligible and the second one is small.

Observations of boundary layer growth in supersonic wind tunnels indicate that, in the Reynolds number range from 5×10^5 to 5×10^6 , and in the Mach number range from 1.5 to 2.5, the boundary layer is turbulent and the displacement thickness grows in proportion to the distance from the throat. This Reynolds number is based on the velocity and kinematic viscosity at the particular station and the distance from the throat to this station. Although the strong cooling of the boundary layer and the much larger pressure gradient in the rocket nozzle would suggest caution in applying wind tunnel results to rocket nozzles, there are some observations in cold flow through rocket-type nozzles which indicate similar behavior. (This conclusion will be utilized in Art. 5 in the discussion of convective heat transfer in rocket nozzles.)

$$\delta^* \text{ (displacement thickness)} \cong 0.004L_n \text{ (distance from throat)} \quad (3-4)$$

With this relation it turns out that the exit area constriction for a 15° half angle nozzle is only 3 per cent. Inspection of Fig. G,2e and G,2f shows that the effect of a 3 per cent area reduction can be neglected if the nozzle area ratio is near the optimum. For narrower exit cones and for off-design nozzles, it may be necessary to allow for this effect.

This is another instance of the remarkable insensitivity of rocket nozzle performance to flow disturbances that are of great importance in wind tunnel nozzle design.

Jet detachment or flow separation. It is not always possible to provide a nozzle with the optimum area ratio for each condition of ambient pressure. In particular, the exhaust nozzle of a rocket airplane that must fly at altitudes from sea level to perhaps 60,000 feet, or of a guided missile that starts at sea level and reaches 100,000 at burnout, generally operates in a very much overexpanded condition at the lower altitudes. The question arises whether the flow in the divergent section remains isentropic.

The possibility of a stationary shock wave perpendicular to the flow axis has been recognized for a long time, and the early literature on rocket performance indicates that this is to be expected. However, although such normal shocks have been observed in supersonic flow channels with small angles of divergence, normal shocks have not been found at all in rocket nozzles. Instead,* it is found that when the back pressure (pressure of the surrounding atmosphere) exceeds the isentropic exit pressure by a large enough amount, the flow separates symmetrically from the nozzle wall, and a complicated pattern of oblique shock waves appears in the stream beyond the point of separation (Plate G,3).

The fundamental fluid mechanics of this type of separation phenome-

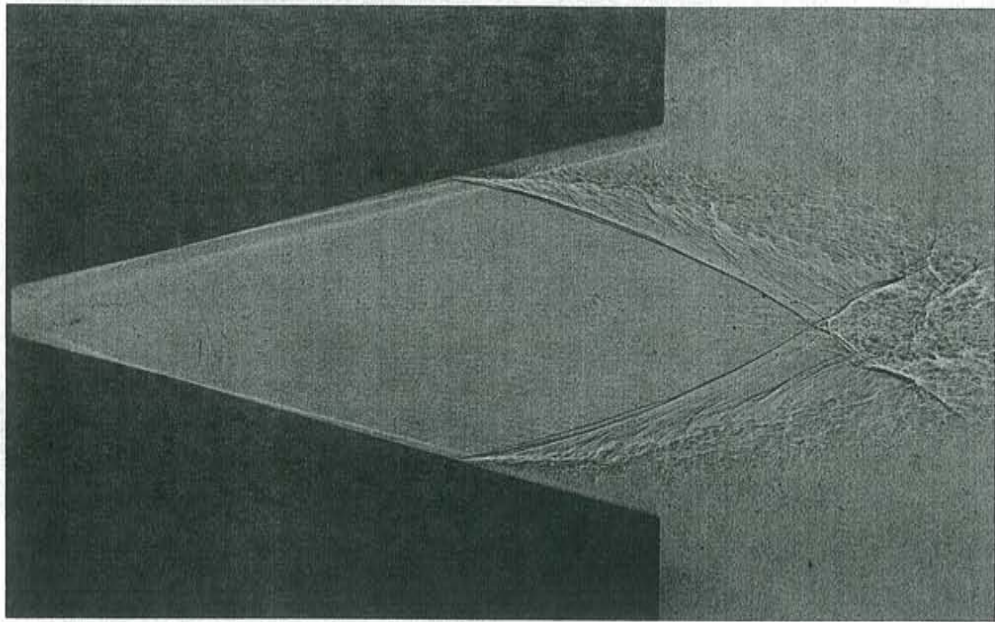


Plate G,3. Spark shadowgraph of flow in overexpanded nozzle.

G,3 · DEPARTURES FROM IDEAL PERFORMANCE

non is discussed in IV,B. In brief, the region of importance is the place near the wall where the shock wave penetrates the boundary layer. Here the sharp adverse pressure gradient connected with the shock thickens the boundary layer and leads to deflection of the flow, while the pressure rise across the shock is supported by the momentum transfer from the

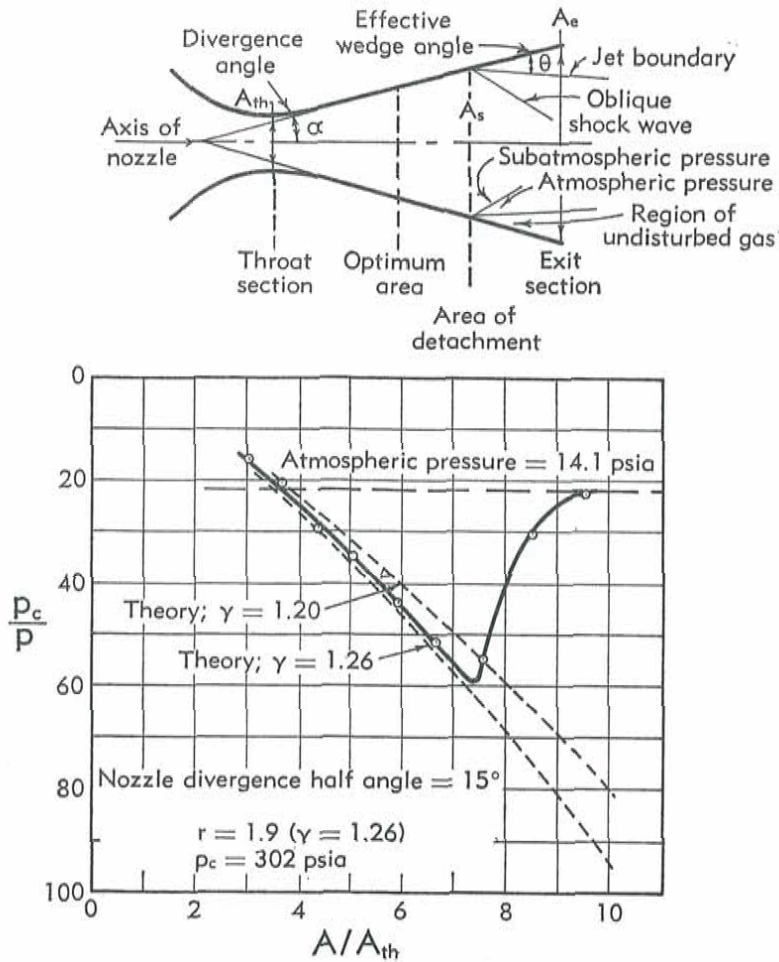


Fig. G,3b. Typical static pressure distribution in exhaust nozzle.

supersonic stream to the "stagnant" fluid in the flow corner. Consequently the strength of the shock and the separation location depend on the state of the boundary layer (laminar or turbulent) and particularly on its development along the nozzle wall prior to separation. For the purpose of the reader interested in rockets, the subject can be presented most usefully in terms of the experimental results and the empirical correlations.

The static pressure distribution in the nozzle is shown in Fig. G,3b. The pressure follows the isentropic expansion curve until the separation

point is reached. At this point, the pressure rises steeply to almost the level of the ambient pressure at the exit, indicating a rather clean break-away of the flow. From the standpoint of thrust, the nozzle may well be cut off at the separation station, since the internal and external pressures are very nearly in balance beyond this point. Experimentally, it makes little difference if a longer nozzle is used, once separation has occurred. The extra length of nozzle does not affect the location of separation and has no appreciable effect on the thrust. (There is a small reduction in thrust due to the extra length of cone, because the internal pressure is slightly less than the external pressure, but this is usually neglected in performance estimates.)

It is obvious that the complicated flow structure downstream of separation is of no consequence in the computation of thrust. The thrust of a rocket motor with separation in the nozzle is calculated on the assumption that the nozzle area ratio is not that corresponding to the actual exit but rather that of the separation station. Therefore it is necessary to be able to predict the location of separation.

In tests with nitric acid-aniline rocket motors employing nozzles with half angles α of 10° , 15° , 20° , and 30° , with actual area ratios ϵ of 10 and 20, and with pressure ratios p_0/p_∞ from 11 to 25, it was found that

$$\frac{p_n}{p_\infty} \cong 0.36 \pm 0.02 \quad (3-5)$$

Almost identical results were obtained at all mixture ratios, and in fact, the results obtained with the nitrogen flow channel previously mentioned were also nearly the same. Consequently, as a general rule for estimating the performance of overexpanded nozzles in the absence of specific test data, the relation (Eq. 3-5) may be used.

Heat loss from the combustion gas. The transfer of heat from the combustion gas to the relatively cold motor walls, by convection and by radiation, affects the performance of the motor. Two cases of heat transfer are of practical interest: (a) the heat transferred is completely removed from the thermodynamic process, as in a water-cooled motor; and (b) the heat is reintroduced into the process as in a motor cooled by the propellants (regenerative cooling). These two processes, together with the adiabatic one, are shown in the h, s diagrams of Fig. G,3c.

In diagram 1, the case of no heat loss, the working fluid (product gas) is injected into the chamber cold at A , is heated adiabatically at constant pressure by combustion to point B , and is expanded isentropically to ambient pressure at C . The enthalpy drop from B to C is transformed to the kinetic energy of the jet (see Eq. 2-10). In diagram 2, the case of heat lost to the cooling water, it is assumed in order to simplify the calculations that the heat removal is concentrated at two stations, the hot end of the chamber and the throat of the exhaust nozzle. (This is reason-

able on the basis of experimental heat transfer distributions.) The process is then as follows: adiabatic combustion from A to B , constant pressure heat loss from B to D , isentropic expansion from D to E , constant pressure heat loss from E to F , and isentropic expansion from F to G . The regenerative process, diagram 3, traces the following path: constant pressure heating from A to J , adiabatic combustion from J to K , heat loss from K to L , expansion from L to M , heat loss from M to N , and expansion from N to O .

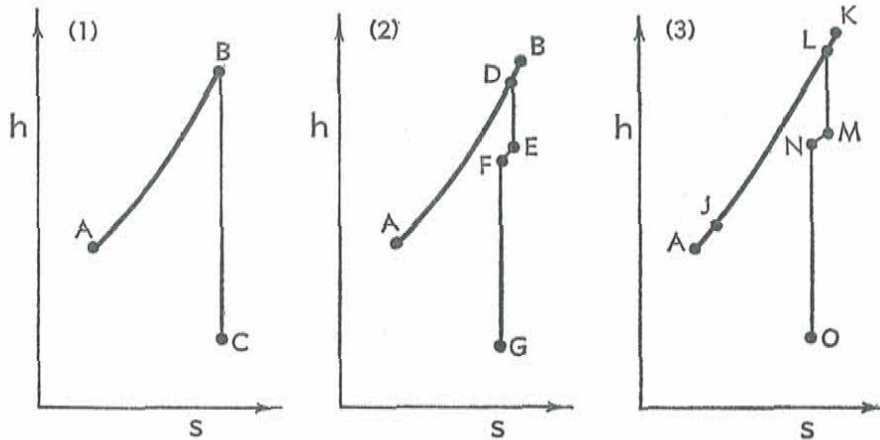


Fig. G,3c. Thermodynamic processes for (1) adiabatic, (2) water-cooled, and (3) regeneratively cooled rocket motors.

The exhaust velocities for the three diagrams are:

$$\left. \begin{aligned} \frac{1}{2} V_{e(1)}^2 &= h_B - h_C \\ \frac{1}{2} V_{e(2)}^2 &= (h_D - h_E) + (h_F - h_G) \\ \frac{1}{2} V_{e(3)}^2 &= (h_L - h_M) + (h_N - h_O) \end{aligned} \right\} \quad (3-6)$$

$$\text{The heat of combustion: } \Delta h_C = h_B - h_A = h_K - h_J \quad (3-7)$$

In cases 2 and 3, the heat transferred per unit mass is given by:

$$\left. \begin{aligned} \Delta q_2 &= (h_B - h_D) + (h_E - h_F) \\ \Delta q_3 &= (h_K - h_L) + (h_M - h_N) = (h_J - h_A) \end{aligned} \right\} \quad (3-8)$$

For a perfect-gas working fluid with constant specific heat, the ratio of the exhaust velocity of the cooled motor to that of the ideal motor can be given explicit form, in each case, in terms of the heat of combustion and the pressure ratio. In general, to calculate the correction with precision, it is necessary to refer to actual h,s computations on diagrams that incorporate the temperature-dependent specific heats and the effects of dissociation. It is immediately evident from the diagrams that the water-cooled motor produces a lower specific impulse than the ideal one. In practice, the approximate formula: $V_{e(2)} \cong V_{e(1)} [(\Delta h_c - \Delta q_2) / \Delta h_c]^{1/2}$ is applied

to relate the two results. For small test motors, this can amount to as much as 5 per cent. It is also evident that the specific impulse of a regeneratively cooled motor is never less than that of the ideal one, and can exceed the ideal performance if the heat transfer $h_M - h_N$ is large in comparison with $h_K - h_L$. In practice, this effect is too small to be measured.

Suspended liquid or solid particles in the exhaust jet. Condensed phases can appear in the exhaust jet if elements are present in the reactants that form refractory products. For example, fuel compounds based on the light metals Li, Be, Al, and Mg produce oxides Li_2O , BeO , Al_2O_3 , and MgO when reacted with oxygen. These oxides have normal vaporization temperatures of 2250, 3900, >1700 , and $>2800^\circ\text{C}$, respectively, and therefore these vapors would condense to droplets or solid particles whenever the temperature drops below these levels, either in the combustion or in the expansion process. Similarly, carbon (sublimation point $>4200^\circ\text{C}$) which can form in large amounts in the decomposition of acetylenic monopropellants, and KCl (sublimation point, 1500°C) which forms in solid propellant combustion where potassium perchlorate is used as the oxidizer, present the problem of flow with condensed phases.

The occurrence of condensation leads to a reduction in specific impulse for two reasons. The portion of the working fluid that condenses cannot perform any expansion work and therefore cannot contribute to the acceleration of the jet; also, the heat in the condensed phase is partly ejected with the jet and not transformed to kinetic energy, because of the low rate of heat transfer from the hot particles to the surrounding gas. The rate of heat transfer depends on the particle size, which in turn depends on whether condensation occurs in the chamber or at some position in the nozzle. Average particle sizes have been observed in the range from 10μ to 50μ .

To analyze the problem in the most exact way, it is necessary to know at what place in the expansion process nucleation occurs, the rate of growth of the condensed nuclei, the rate of heat transfer from the hot particles to the cooler gas stream, and the velocity lag between the suspended particles and the gas stream. For practical purposes, it is usually adequate to simplify the analysis by assuming that the velocity lag is zero. Concerning heat transfer, two extreme assumptions are possible: (1) the temperature of the condensed phase remains the same throughout the expansion process as that of the gas where condensation took place, that is, zero heat transfer; and (2) the condensed phase temperature follows exactly the temperature history of the gas, that is, perfect heat exchange. The first assumption would apply to very large particles; the second assumption would apply to very small particles.

The equation of state of the mixture of gas and suspended particles, and the density of the mixture ρ , are definable in terms of the mean

G,3 · DEPARTURES FROM IDEAL PERFORMANCE

molecular weight \mathfrak{M}_g of the gas, the molecular weight of the solid \mathfrak{M}_s , the mean molecular weight of the mixture $\overline{\mathfrak{M}}$, and the respective numbers of moles of gas and solid, n_g and n_s , in a standard molar volume \mathcal{U}_0 .

$$\left. \begin{aligned} p &= \frac{n_g}{\mathcal{U}_0} RT_g = p_g \\ \rho &= \frac{n_s \mathfrak{M}_s + n_g \mathfrak{M}_g}{\mathcal{U}_0} \end{aligned} \right\} \quad (3-9)$$

For adiabatic, frictionless flow, $dh = (1/\rho)dp$. For the mixture,

$$\frac{n_g C_{p_g} dT_g + n_s C_{p_s} dT_s}{n_g \mathfrak{M}_g + n_s \mathfrak{M}_s} = \frac{n_g RT_g}{n_g \mathfrak{M}_g + n_s \mathfrak{M}_s} \frac{dp_g}{p_g} \quad (3-10)$$

Introducing mole fractions X_g and X_s , this equation becomes

$$X_g C_{p_g} \frac{dT_g}{T_g} + X_s C_{p_s} \frac{dT_s}{T_s} = X_g R \frac{dp_g}{p_g} \quad (3-11)$$

For adiabatic flow, $VdV + dh = 0$. For the mixture, with zero velocity lag,

$$\frac{1}{2}(X_g \mathfrak{M}_g + X_s \mathfrak{M}_s) VdV + X_g C_{p_g} dT_g + X_s C_{p_s} dT_s = 0 \quad (3-12)$$

Eq. 3-11 and 3-12 are applicable upstream of the condensation location, if X_g is set equal to unity, and X_s equal to zero. Downstream of this location, these equations can be applied if it is assumed that the mole fractions X_g and X_s are fixed. This is a reasonable assumption since most of the condensation takes place in a very short region.

A satisfactory solution of the problem is to obtain V_e in terms of the pressure ratio p_e/p_o . This can be obtained by integrating Eq. 3-11 and 3-12 if the ratio dT_s/dT_g can be specified. For case 1 mentioned above, the ratio is zero; for case 2, the ratio is unity; and other cases can be treated. The most extreme case is to assume that dT_s/dT_g is zero and that condensation occurs in the combustion chamber, so that the particles are at temperature T_o at the exit. This leads to:

$$\begin{aligned} V_e &= \left\{ \frac{2X_g C_{p_g} T_o}{\overline{\mathfrak{M}}} \left[1 - \left(\frac{p_e}{p_o} \right)^{\frac{\gamma-1}{\gamma}} \right] \right\}^{\frac{1}{2}} \\ \overline{\mathfrak{M}} &= X_g \mathfrak{M}_g + X_s \mathfrak{M}_s \\ \gamma &= C_{p_g} / C_{v_g} \end{aligned} \quad (3-13)$$

For a typical propellant gas composition, based on hydrocarbon combustion, the condensation of 20 per cent of the mass in the combustion chamber leads to about 10 per cent loss in I_{sp} , by formula (Eq. 3-13). The effect can therefore be of considerable importance for some propellant systems.